systems are needed before contemplating the use of this technique for cell therapy. In addition, the mechanisms governing the differentiation of human tissues must be elucidated in order to produce tissue-specific cell populations from undifferentiated ES cells. This study shows the feasibility of generating human ES cells from a somatic cell isolated from a living person.

References and Notes

1. J. A. Thomson *et al*., *Science* **282**, 1145 (1998).
2. D. Solter, *Nature Rev. Genet.* **1**, 199 (2000).
3. R. P. Lanza, J. B. Cibelli, M. D. West, *Nature Med.* **5**, 975 (1999).
4. J. B. Cibelli *et al*. *Nature Biotechnol*. **16,** 642 (1998).
5. M. J. Munsie *et al*., *Curr. Biol.* **10**, 989 (2000).
6. E. Kawase, Y. Yamazaki, T. Yagi, R. Yanagimachi, R. A. Pederson, *Genesis* **28**, 156 (2000).
7. T. Wakayama *et al*., *Science* **292**, 740 (2001).
8. J. B. Cibelli *et al.*, *J. Regen. Med.* **26**, 25 (2001).
9. Y. Shu, G. Zhuang, *Fertil. Steril.* **78**, S286 (2002).
10. Materials and methods are available as supporting material on *Science* Online.
11. J. Kwun *et al*., *Mol. Reprod. Dev.* **65**, 167 (2003).
12. S. H. Hyun *et al*., *Biol. Reprod.* **69**, 1060 (2003).
13. B. Kuhholzer, R. J. Hawley, L. Lai, D. Kolber-Simonds, R. S. Prather, *Biol. Reprod.* **64**, 1635 (2004).
14. M. H. Kaufman, *Nature* **242**, 475 (1973).
15. K. Nakagawa *et al*., *Zygote* **9**, 83 (2001).
16. D. K. Gardner, M. Lane, W. B. Schoolcraft, *J. Reprod. Immunol.* **55**, 85 (2002).
17. A. Langendonckt, D. Demylle, C. Wyns, M. Nisolle, J. Donnez, *Fertil. Steril.* **76**, 1023 (2001).
18. Y. H. Choi, B. C. Lee, J. M. Lim, J. M. S. K. Kang, W. S. Hwang, *Theriogenology* **58**, 1187 (2002).
19. D. K. Barnett, B. D. Bavister, *Mol. Reprod. Dev.* **43**, 105 (1996).
20. S. H. Lee, N. Lumelsky, L. Studer, J. M. Auerbach, R. D. Mckay, *Nature Biotechnol.* **18**, 675 (2000).
21. F. Mitelman, *An International System for Human Cytogenetic Nomenclature* (S. Karger, Basel, Switzerland, 1995).
22. J. A. Thomson *et al*., *Proc. Natl. Acad. Sci. U.S.A.* **92**, 7844 (1995).
23. B. E. Reubinoff, F. P. Pera, C.-Y. Fong, A. Trounson, A. Bongso, *Nature Biotechnol.* **18**, 399 (2000).
24. S. R. John, *Trends Biotechnol.* **20**, 417 (2002).
25. K. E. Vrana *et al*., *Proc. Natl. Acad. Sci. U.S.A.* **100** (suppl. 1), 1911 (2003).
26. C. Simerly *et al*., *Science*, **300**, 297 (2003).
27. I. Wilmut *et al.*, *Nature* **385**, 810 (1997).
28. D. Humphreys *et al*., *Proc. Natl. Acad. Sci. U.S.A.* **99**, 12889 (2002).
29. S. E. Lanzendorf *et al*., *Fertil. Steril.* **76**, 132 (2001).

30. We thank Y. Y Hwang (Hanyang University) for assistance with oocyte collections; S. I. Rho (MizMedi Hospital), H. S. Yoon (MizMedi Hospital,) and S. K. Oh (Seoul National University) for assistance on hES cells culture; Y. K. Choi (Korea Research Institute of Bioscience and Biotechnology) for assistance on teratoma formation; Tak Ko (Michigan State University) for gene expression analysis of Cyno-1 cells; and A. Trounson (Monash University), B. D. Bavister (University of New Orleans), and D. P. Wolf (Oregon National Primate Research Center) for critical review of the manuscript. J. B. Cibelli made intellectual contributions to the manuscript and the RNA analysis of nonhuman primate cells. All human experiments were performed in Korea by Korean scientists. This study was supported by grants from Advanced Backbone IT Technology Development (grant IMT2000-C1-1) to W.S.H. and the Stem Cell Research Center (grant M102KL0100-02K1201-00223) to S.Y.M. The authors are grateful for a graduate fellowship provided by the Ministry of Education through the BK21 program.

Supporting Online Material

www.sciencemag.org/cgi/content/full/1094515/DC1
Materials and Methods
SOM Text
Fig. S1

9 December 2003; accepted 4 February 2004
Published online 12 February 2004;
10.1126/science.1094515
Include this information when citing this paper.

Force-Clamp Spectroscopy Monitors the Folding Trajectory of a Single Protein

Julio M. Fernandez* and Hongbin Li

We used force-clamp atomic force micoscopy to measure the end-to-end length of the small protein ubiquitin during its folding reaction at the single-molecule level. Ubiquitin was first unfolded and extended at a high force, then the stretching force was quenched and protein folding was observed. The folding trajectories were continuous and marked by several distinct stages. The time taken to fold was dependent on the contour length of the unfolded protein and the stretching force applied during folding. The folding collapse was marked by large fluctuations in the end-to-end length of the protein, but these fluctuations vanished upon the final folding contraction. These direct observations of the complete folding trajectory of a protein provide a benchmark to determine the physical basis of the folding reaction.

Resolving the folding pathway of a protein remains a challenge in biology (*1*–*9*). Here, we demonstrate a method by which the entire folding trajectory of a single protein can be recorded as a function of time. We used single-molecule atomic force micoscopy techniques (*10*, *11*) in the force-clamp mode (*12*, *13*) to apply a constant force to a single polyprotein composed of nine repeats of the small protein ubiquitin (*13*–*16*). This resulted in the probabilistic unfolding of ubiquitin, which was observed as stepwise elongations of the protein in which each step corresponded to the unfolding of an individual protein module (*12*). We applied this technique to monitor the end-to-end length of a single ubiquitin polyprotein (*17*) during reversible unfolding-folding cycles. Our experimental approach is illustrated in Fig. 1. Figure 1A shows the changes in the length of a single ubiquitin polyprotein in response to the stretching force displayed in Fig. 1B. As shown, stretching the polyubiquitin chain at 120 pN triggers a series of unfolding events that appear as a staircase of 20-nm steps, marking the unfolding of the individual ubiquitins in the chain (Fig. 1A). After 4 s, the force was relaxed to 15 pN (Fig. 1B) (*18*), and we observed the protein spontaneously contract in stages until it reached its folded length (Fig. 1A). To confirm that the polyprotein had folded, we raised the stretching force back to 120 pN at 14 s (Fig. 1B) and observed the ubiquitin chain extend in steps of 20 nm back to its fully unfolded length (Fig. 1A). Hence, the spontaneous contraction of the protein observed upon reducing the force from 120 pN down to 15 pN corresponds to the folding trajectory of the mechanically unfolded ubiquitin.

We observed and analyzed 81 folding events similar to those shown in Fig. 1. Two typical folding trajectories for mechanically unfolded polyubiquitin molecules are shown in Fig. 2. Most of the folding trajectories are qualitatively similar, following a continuous convex time course marked by abrupt changes in slope. However, we have never observed identical sets of trajectories, indicating the existence of multiple folding pathways for ubiquitin. To simplify the analysis of the folding trajectories, we divided their time course, roughly, into four distinct stages marked by abrupt changes in the slope of the collapse (Fig. 2). As an example, we analyze the recording shown in Fig. 2A. The first stage (1 in Fig. 2A and inset) is fast, lasting ~10 ms, which is slower than the time it takes the force to reach its set point (~3 ms in this experiment). The collapse rate for this stage (cr_1 = 2135 nm/s) is within the range but clearly slower than the maximum rate of change, or slew rate (*sr*), of the feedback during this experiment (measured at *sr* = ~8300 nm/s, after the molecule detached from the cantilever). This stage is likely to correspond to the elastic recoil of the unfolded polypeptide chain adjusting its length to the step change in the pulling force. This stage is always fast and is clearly marked in

Department of Biological Sciences, Columbia University, New York, NY 10027, USA.

*To whom correspondence should be addressed. E-mail: jfernandez@columbia.edu

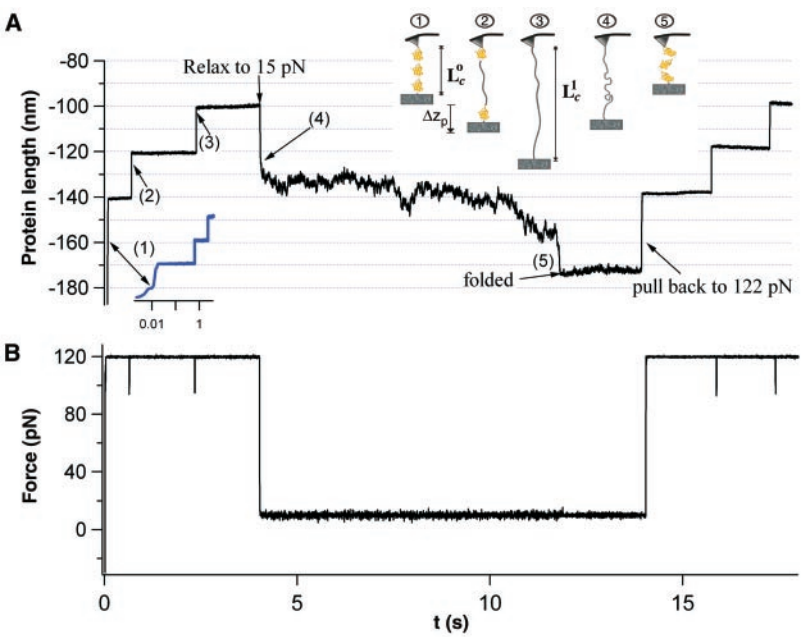

Fig. 1. The folding pathway of ubiquitin is directly measured by force-clamp spectroscopy. The figure shows our experimental protocol. (**A**) The end-to-end length of a protein as a function of time. (**B**) The corresponding applied force as a function of time. The inset in (A) shows a schematic of the events that occur at different times during the stretch-relaxation cycle (numbered from 1 to 5). Δz_p, piezoelectric actuator displacement; L_c, contour length. The length of the protein (in nanometers) evolves in time as it first extends by unfolding at a constant stretching force of 122 pN. This stage is characterized by step increases in length of 20 nm each, marking each ubiquitin unfolding event, numbered 1 to 3. The first unfolding event (1) occurred very close to the beginning of the recording and therefore it is magnified with a logarithmic time scale (blue inset) with the length dimension plotted at half scale. Upon quenching the force to 15 pN, the protein spontaneously contracted, first in a steplike manner resulting from the elastic recoil of the unfolded polymer (4), and then by a continuous collapse as the protein folds (5). The complex time course of this collapse in the protein's length reflects the folding trajectory of ubiquitin at a low stretching force. To confirm that our polyubiquitin had indeed folded, at 14 s we stretched again back to 122 pN (B). The initial steplike extension is the elastic stretching of the folded polyubiquitin. Afterward, we observed steplike extension events of 20 nm each, corresponding to the unfolding of the ubiquitin proteins that had previously refolded. After these unfolding events, the length of the polyubiquitin is the same as that measured before the folding cycle began (3).

all recordings. The second stage begins at the end of the rapid elastic recoil and is marked by a noticeable increase in length fluctuations (Fig. 2A, inset). This stage relaxes into a long-lasting plateau with a slow rate of collapse measured at $cr_2 = 4.3$ nm/s. The beginning of the third stage in this recording is distinguished by an abrupt increase in the slope of the collapse that now measures $cr_3 = 43$ nm/s. Stages 2 and 3 can vary greatly in their rates of collapse (Fig. 3) and cannot always be distinguished (fig. S1). The final stage of collapse is always fast and appears almost steplike in most recordings. However, upon close inspection, the final stage is continuous and has a finite collapse rate of only $cr_4 = 1100$ nm/s in the recording shown in Fig. 2A, and it is far from an all-or-none steplike event. This final stage (stage 4) is well defined in most recordings, with an average slope of $cr_4 = 585 \pm 552$ nm/s ($\pm$SD; $n = 46$).

A notable feature of the folding collapse is that stages 2 and 3 show very large fluctuations of the end-to-end length of the protein (~16 nm peak to peak in the inset of Fig. 2B). The magnitude of these fluctuations abates quickly upon folding, as shown by the amplitude of the fluctuations in regions II and III of Fig. 2B. Although in this example the fluctuations appear relatively constant in region II, we also observed several cases in which the fluctuations grew in amplitude toward the end of region II and then disappeared upon folding. A detailed analysis of these fluctuations is beyond the scope of this work. Part of these length fluctuations must result from noise in the force signal, which becomes amplified by the increased slope of the length-force relationship at low pulling forces. However, it is hard to avoid the conclusion that most of these fluctuations represent a fundamental property of the unfolded polypeptide when it nears its final folding collapse. Although nearly all of the folding trajectories appear continuous and the stages

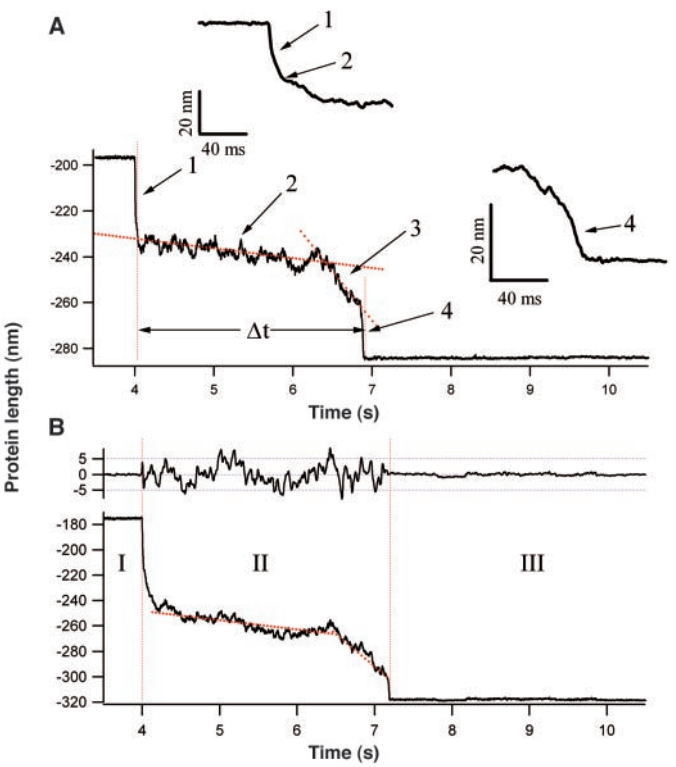

Fig. 2. Folding is characterized by a continuous collapse rather than by a discrete all-or-none process. (A) and (B) show typical recordings of the time course of the spontaneous collapse in the end-to-end length of an unfolded polyubiquitin, observed after quenching to a low force. (**A**) Four distinct stages can be identified. The first stage is fast and we interpret it as the elastic recoil of an ideal polymer chain (see magnified trace in the top inset). The next three stages are marked by abrupt changes in slope and correspond to the folding trajectory of ubiquitin. These stages can be distinguished by their different slopes. Stages 2 and 3 always show peak-to-peak fluctuations in length of several nanometers. The rapid final contraction of stage 4 marks the end of the folding event. This final collapse stage is not instantaneous, as can be seen on the magnified trace in the lower inset. We measure the total duration of the collapse, Δt, from the beginning of the quench until the end of stage 4. (**B**) The folding collapse is marked by large fluctuations in the length of the protein. These fluctuations greatly diminish in amplitude after folding is complete. The inset at the top is a record of the end-to-end fluctuations of the protein before the quench (region I), during the folding collapse (region II), and after folding was completed (region III). The fluctuations were obtained by measuring the residual from linear fits to the data (red dotted lines).

of collapse are marked by abrupt changes in slope (Fig. 2), in 1 case out of 81 folding trajectories we observed a stepwise folding collapse (fig. S2). However, in this recording, only two ubiquitin modules refolded in three well-separated steplike events.

The total duration of a folding trajectory (Δt in Fig. 2A) is dependent on the stretching force. Figure 3 shows four folding trajectories at different forces. The downward arrows mark the time point when the stretching force was quenched to a low value (20 to 50 pN, Fig. 3). The immediate shortening of the protein's length marked by the downward arrows corresponds to the elastic recoil (stage 1, Fig. 2A), which is proportional to the magnitude of the quench (*18*).

A shallow quench to 50 pN fails to trigger folding, showing only stages 1 and 2 of a folding trajectory (Fig. 3A). In 51 recordings that showed trajectories that only reached stage 2, we never observed folding events (282 unfolding events, 0 folding events; fig. S3). By contrast, in 31 recordings in which the folding trajectories were interrupted at stage 3, folding became detectable (154 unfolding events, 11 folding events; fig. S4). In some of these trajectories that failed to fold, large fluctuations in the end-to-end length of the protein of more than 30 nm were observed throughout (trace 3 in fig. S4). As the magnitude of the quench grows, complete folding trajectories begin to appear and become shorter (35 pN, Fig. 3, B and C; 23 pN, Fig. 3D). The upward-pointing arrow marks the point at which the high stretching force was restored (100 to 120 pN, Fig. 3). After the high stretching force is restored, the ubiquitin chain regains the original unfolded length either very fast when it had failed to fold (simple elastic stretching, Fig. 3A; figs. S3 and S4) or more slowly through a staircase of 20-nm steps marking the unfolding of the refolded ubiquitins (Fig. 3, B to D).

From a series of experiments such as those shown in Fig. 3, we have determined that the collapse time is dependent on the pulling force applied during folding and also on the contour length of the unfolded polypeptide (Fig. 4). For example, at a stretching force of 30 to 40 pN, the folding time correlates with the unfolded contour length as $\Delta t \cong 0.027 \times L_u$ (Fig. 4A). The slope of the time versus length curve is strongly dependent on the force applied during the folding collapse (Fig. 4A). However, because the folding time depends on the contour length as well, we plot the folding time as a function of force for proteins that have a contour length in the range of 150 to 200 nm (Fig. 4B). We can describe the force (F) dependency of the folding time by a simple exponential function as $\Delta t \cong 0.01 \times \exp(F \times 0.2)$ (solid line in Fig. 4B). Both the length and force dependency can be approximated by $\Delta t \cong 3 \times 10^{-5} \times L_u \times \exp(F \times 0.2)$. This description is far from unique, because in the absence of an explicit physical model for the folding collapse, the choice of any given function is arbitrary. Nonetheless, it is interesting to consider that models of polymer collapse predict that the time of collapse depends on the contour length of the polymer (*19*, *20*). Resolving the exact form of the force and length dependency of the collapse will require a substantially improved set of data with less scatter. For example, for a quench to about 20 to 30 pN and at a relatively constant contour length (Fig. 4; 90 to 120 nm), the folding times range between 120 ms and up to ~3 s. However, it is unclear whether this scatter is the result of different sets of folding trajectories that take very different times to resolve into an actual folding event or is due to experimental error.

We did not control the site from which we picked up the protein, and therefore, we obtained a random sample of single molecules containing anywhere between one and nine repeats (*21*). In most cases, we picked up three- to five-long ubiquitin chains, but we could easily obtain chains of up to seven (Fig. 3). In a few occasions (n = 5), we observed the folding trajectory for only one ubiquitin (Fig. 5). In these cases, we observed the same stages of collapse as before, except that the difference between stages 3 and 4 appeared to be discrete fluctuations in length that are sometimes clearly observed before the occurrence of stage 4 (Fig. 5, top two recordings). It is also notable that the final stage of the folding collapse is still rate-limited (Fig. 5, 160 nm/s in the top inset and 194 nm/s in the bottom inset) and much slower than the slew rate of the force clamp in those recordings (~6000 nm/s; Fig. 5).

In contrast with the steplike folding reactions of an RNA hairpin placed under a stretching force (*22*), our measurement of the folding trajectories of mechanically unfolded proteins revealed a more complex phenomenon. Initially the collapse is very fast, driven by the elastic recoil, but then it is arrested into a slow stage that can take up to several seconds to resolve.

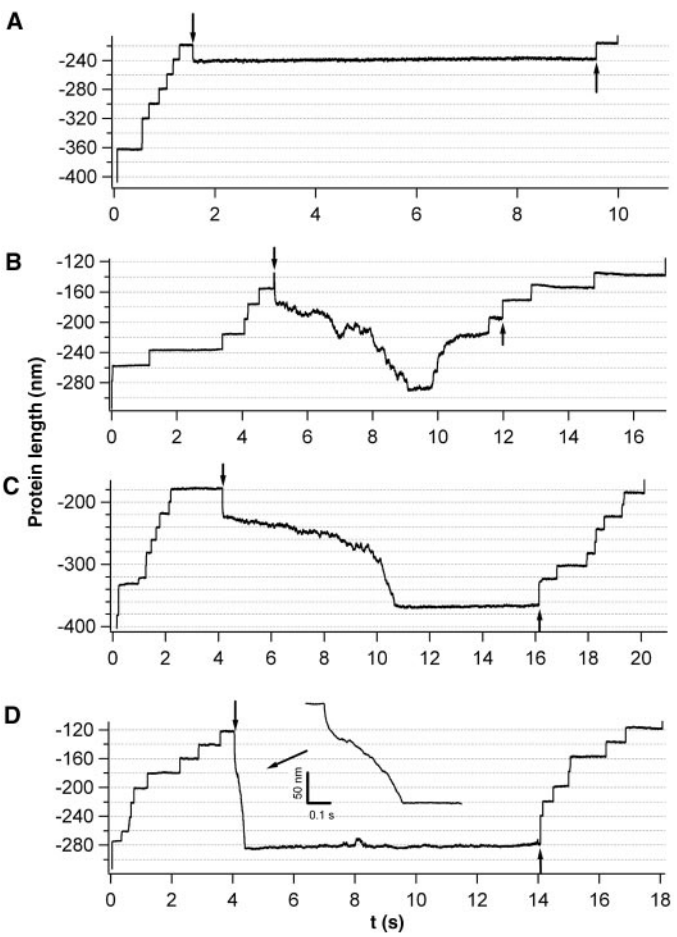

Fig. 3. The duration of the folding collapse is force dependent. We show four different traces from ubiquitin chains for which we observed seven unfolding events (recorded at 100 to 120 pN) before relaxing the force. Hence, the unfolded length of all these recordings is comparable. (**A**) In the first recording, the force was quenched to ~50 pN (downward arrow). An instantaneous elastic recoil was observed. However, the ubiquitin chain fails to fold, as evidenced by its constant length at this force. Upon restoration of a high stretching force (120 pN, upward arrow), the ubiquitin chain is observed to elastically extend back to its fully unfolded length. (**B** and **C**) Recordings similar to that shown in (A) (seven initial unfolding events), in which the force was quenched further down to ~35 pN. In contrast to (A), the length of the ubiquitin chain was observed to spontaneously contract to the folded length. In (B), the folded ubiquitin chain was observed to unfold partially at the low force, whereas in (C) it remains folded until the high stretching force is restored (upward arrow). Several unfolding events mark this last stage, bringing the ubiquitin chain back to its unfolded length. (**D**) A case in which the force was quenched even further down to 23 pN. In this case, the folding collapse was completed in much less time (inset), clearly showing that the probability of observing a folding event as well as its duration is strongly force dependent.

At first glance, this suggests an intermediate state in the folding pathway (*23*). Indeed, ubiquitin is proposed to have such an intermediate (*14*). However, given that the slow stage of the collapse appears to be highly cooperative and lacks the features of Markovian kinetics, describing this stage as a kinetic intermediate may not be correct. Indeed, the time course of the observed folding trajectories is very different from those expected of a simple two-state folding reaction, which should be marked by stepwise shortening events as the individual ubiquitin proteins fold in the chain. Furthermore, the folding events are expected to occur stochastically, and hence they should be well separated in time. By contrast, the observed time course of the folding trajectory appears to be cooperative, in which most of the ubiquitin proteins in the chain follow similar folding stages at the same time. This is hard to explain unless the unfolded protein is behaving at least partially as a single polymer chain collapsing cooperatively.

Single-molecule force spectroscopy affords a high degree of control over the conformation of a protein. For example, stretching a fully unfolded ubiquitin chain by ~100 to 120 pN causes the polypeptide to extend by >85 to 90% of its contour length (*15*). At these extensions, most or all of the secondary structure of a protein will be unraveled. Hence, the starting point of the folding trajectory is well defined as the point where the protein has been forced into a state in which all of the residues are exposed to the saline solution. Under these conditions, the unfolded ubiquitin chain can be considered as a polymer coil that is placed in a poor solvent. It is well known that polymers placed in a poor solvent undergo rapid collapse from a random coil into a condensed globular form [the so-called "coil-globule" phase transition (*19*, *20*, *24–28*)]. Polymer collapse has been shown to occur in distinct stages that are qualitatively similar to the protein-folding trajectories demonstrated here (*29*). Furthermore, the large fluctuations in the end-to-end length of the protein that we observed in the folding trajectories are a characteristic of critical phenomena and have been observed in polymer chains just before undergoing a coil-globule phase transition. (*30*) Hence, the various stages of the folding collapse described here (stages 2, 3, and 4; Fig. 2) may correspond to those of a polymer undergoing a coil-globule phase transition. If this view is correct, the folding trajectories of all mechanically unfolded proteins will be very similar and would be identical to those of nonfolding polymers placed into a poor solvent solution. From this perspective, a folding transition state could only be reached after the end of stage 4 (Fig. 2). However, we know that ubiquitin folding is already observed in stage 3 of the folding trajectories (fig. S4B). Hence, it is premature to ascribe the folding trajectories that we observed solely to a polymer collapse mechanism (*19*, *20*, *24–28*). Furthermore, simple polymer collapse would lead to a structureless condensed state that would include all of the unfolded ubiquitins in the chain. It is unlikely that only then, each unfolded ubiquitin would begin to search for its native conformation. The folding trajectories shown here are likely to be a more complex phenomenon in which the collapsing polypeptide rapidly begins to form bonds that limit the degrees of freedom of the collapsing chain, guiding the trajectory to the native state. For example, an all-atom

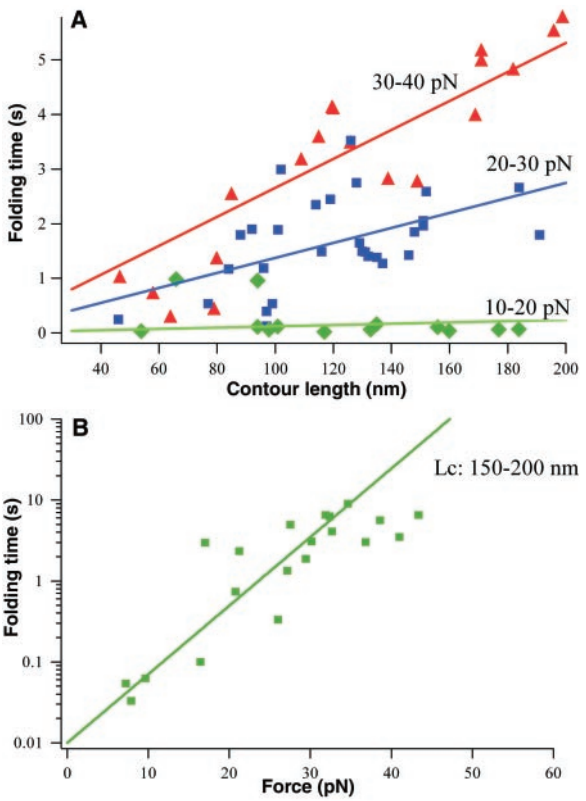

Fig. 4. The duration of the folding collapse is dependent on the protein length and the magnitude of the quench. The duration of the spontaneous collapse of an unfolded ubiquitin chain (Δt; Fig. 2A) depends on the total contour length of the mechanically unfolded polypeptide (**A**) and on the magnitude of the stretching force during refolding (**B**). (A) Three sets of recordings grouped by force range (10 to 20 pN, 20 to 30 pN, and 30 to 40 pN) and plotted against their contour length. The solid lines are linear fits to each set of data with values of 27 ms/nm (red line; 30 to 40 pN), 14 ms/nm (blue line; 20 to 30 pN), and 1.2 ms/nm (green line; 10 to 20 pN). To observe the force dependency we grouped the data from (A) at the highest range of contour lengths for which the effect of the force is most evident (150 to 200 nm). We observed that the duration of the folding collapse is exponentially dependent on the force (B), based on the equation $\Delta t \cong 0.01 \times \exp(F \times 0.2)$ (green line).

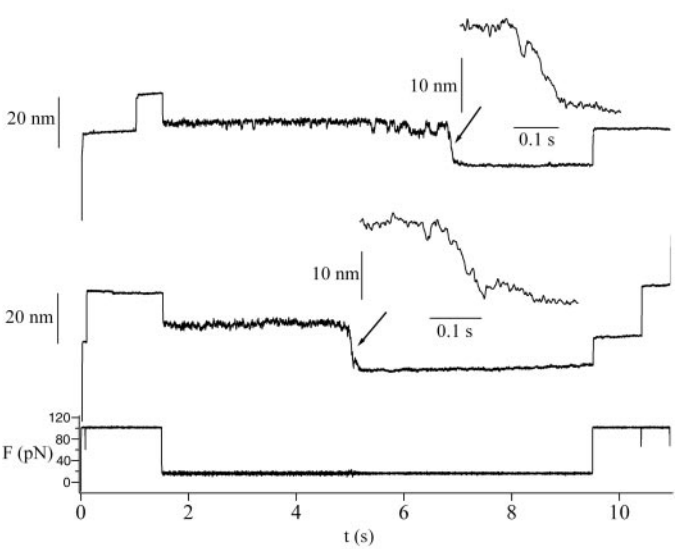

Fig. 5. Two recordings of protein length (nm) as a function of time, showing the folding trajectory of a single ubiquitin. As before, stretching at a high force (100 pN) is followed by a quench to a low force of 26 pN that lasts 8 s, followed by restoration of the high stretching force up to 100 pN (bottom trace). In both cases, a single ubiquitin was observed to unfold at 100 pN. After the quench, the proteins undergo a spontaneous collapse into the folded state. Upon restretching, the folded ubiquitin is observed to elastically extend back to its folded length at 100 pN and then to unfold (second recording). Discrete fluctuations of several nanometers can be observed shortly before the final folding contraction. The final contraction occurred much faster than the previous stage; however, it had a finite rate (**insets**).

simulation showed that the refolding pathway of a protein that had been mechanically stretched into a partially unfolded state involved the formation and rupture of specific hydrogen bonds (*8*). Lattice simulations have predicted that the radius of gyration (related to the end-to-end length) of a folding protein could follow a multiplicity of pathways with a time course that occurs in distinct stages (*31*). More recent simulations have predicted that after a rapid polymer collapse into a semicompact globule, the rate-limiting step for protein folding becomes the random search for any of thousands of transition states that can be reached from this semicompact form. Once a transition state is found, a rapid folding collapse ensues (*4*, *23*, *32*). This folding time course qualitatively reproduces the folding trajectories that we observed.

The direct observation of the folding trajectory of ubiquitin demonstrated here opens the way for a detailed study of protein-folding pathways. Our results contradict the generally held view that folding and unfolding reactions correspond to transitions between well-defined discrete states. In contrast, we observed that ubiquitin folding occurs through a series of continuous stages that cannot be easily represented by state diagrams. By studying how the folding trajectories respond to a variety of physical-chemical conditions (*33*), mutagenesis, and protein engineering (*34*), we may begin to identify the physical phenomena underlying each stage in these protein-folding trajectories.

References and Notes

1. U. Mayor *et al*., *Nature* **421**, 863 (2003).
2. A. Matouschek, J. T. Kellis Jr., L. Serrano, A. R. Fersht, *Nature* **340**, 122 (1989).
3. B. Schuler, E. A. Lipman, W. A. Eaton, *Nature* **419**, 743 (2002).
4. A. Sali, E. Shakhnovich, M. Karplus, *Nature* **369**, 248 (1994).
5. C. Hardin, M. P. Eastwood, M. Prentiss, Z. Luthey-Schulten, P. G. Wolynes, *J. Comput. Chem.* **23**, 138 (2002).
6. K. A. Dill, H. S. Chan, *Nature Struct. Biol.* **4**, 10 (1997).
7. C. M. Dobson, A. Sali, M. Karplus, *Angew. Chem. Int. Ed.* **37**, 868 (1998).
8. M. Gao, H. Lu, K. Schulten, *Biophys. J.* **81**, 2268 (2001).
9. E. Rhoades, E. Gussakovsky, G. Haran, *Proc. Natl. Acad. Sci. U.S.A.* **100**, 3197 (2003).
10. M. Rief, M. Gautel, F. Oesterhelt, J. M. Fernandez, H. E. Gaub, *Science* **276**, 1109 (1997).
11. M. Rief, F. Oesterhelt, B. Heymann, H. E. Gaub, *Science* **275**, 1295 (1997).
12. A. F. Oberhauser, P. K. Hansma, M. Carrion-Vazquez, J. M. Fernandez, *Proc. Natl. Acad. Sci. U.S.A.* **98**, 468 (2001).
13. Materials and methods are available as supporting material on *Science* Online.
14. S. Khorasanizadeh, I. D. Peters, H. Roder, *Nature Struct. Biol.* **3**, 193 (1996).
15. M. Carrion-Vazquez *et al*., *Nature Struct. Biol.* **10**, 738 (2003).
16. M. Carrion-Vazquez *et al*., *Proc. Natl. Acad. Sci. U.S.A.* **96**, 3694 (1999).
17. S. Vijay-Kumar, C. E. Bugg, W. J. Cook, *J. Mol. Biol.* **194**, 531 (1987).
18. The use of a greatly improved piezoelectric actuator together with soft cantilevers makes it possible to control the force and the length of a single protein with pico-Newton and nanometer resolution. However, it is still somewhat difficult to set the exact value of a low-force setting because our current force-clamp apparatus can be affected by small direct current offsets that affect our zero-force set point. These offsets do not affect our results at high stretching forces but can cause an unknown error when quenching the stretched protein to a low force. One way to independently measure the actual quenched force is to measure the magnitude of the elastic recoil that occurs immediately after relaxing the unfolded polymer chain to the lower force (e.g., steplike relaxation that coincides with downward arrows in Fig. 3). Given that in each case we know the contour length of the unfolded polypeptide, we used the wormlike chain model of polymer elasticity to find the magnitude of the force quench for each elastic recoil event.
19. P. G. de Gennes, *J. Phys. Lett. (Paris)* **46**, L639 (1985).
20. A. Y. Grosberg, S. K. Nechaev, E. I. Shakhnovich, *J. Phys. (Paris)* **49**, 2095 (1988).
21. H. Li, A. F. Oberhauser, S. B. Fowler, J. Clarke, J. M. Fernandez, *Proc. Natl. Acad. Sci. U.S.A.* **97**, 6527 (2000).
22. J. Liphardt, B. Onoa, S. B. Smith, I. J. Tinoco, C. Bustamante, *Science* **292**, 733 (2001).
23. Y. Zhou, M. Karplus, *J. Mol. Biol.* **293**, 917 (1999).
24. C. Williams, F. Brochard, H. L. Frisch, *Annu. Rev. Phys. Chem.* **32**, 433 (1981).
25. V. S. Pande, A. Y. Grosberg, T. Tanaka, *Rev. Mod. Phys.* **72**, 259 (2000).
26. A. Buguin, F. BrochardWyart, P. G. deGennes, *C. R. Acad. Sci. Paris* **322**, 741 (1996).
27. A. Halperin, P. M. Goldbart, *Phys. Rev. E* **61**, 565 (2000).
28. T. Frisch, A. Verga, *Phys. Rev. E* **65**, 041801 (2002).
29. B. Chu, Q. C. Ying, A. Y. Grosberg, *Macromolecules* **28**, 180 (1995).
30. I. Nishio, G. Swislow, S. T. Sun, T. Tanaka, *Nature* **300**, 243 (1982).
31. C. J. Camacho, D. Thirumalai, *Proc. Natl. Acad. Sci. U.S.A.* **90**, 6369 (1993).
32. Y. Zhou, M. Karplus, *Nature* **401**, 400 (1999).
33. D. K. Klimov, D. Thirumalai, *Phys. Rev. Lett.* **79**, 317 (1997).
34. S. Nauli, B. Kuhlman, D. Baker, *Nature. Struct. Biol.* **8**, 602 (2001).

35. We thank L. Li and K. Walther for helpful discussions and H. Huang for technical assistance. This work is funded by grants from NIH (J.M.F.).

Supporting Online Material

www.sciencemag.org/cgi/content/full/303/5664/1674/DC1
Materials and Methods
Figs. S1 to S4
References

14 October 2003; accepted 2 February 2004

Columnar Architecture Sculpted by GABA Circuits in Developing Cat Visual Cortex

Takao K. Hensch[1,2]* and Michael P. Stryker[2]

The mammalian visual cortex is organized into columns. Here, we examine cortical influences upon developing visual afferents in the cat by altering intrinsic γ-aminobutyric acid (GABA)–mediated inhibition with benzodiazepines. Local enhancement by agonist (diazepam) infusion did not perturb visual responsiveness, but did widen column spacing. An inverse agonist (DMCM) produced the opposite effect. Thus, intracortical inhibitory circuits shape the geometry of incoming thalamic arbors, suggesting that cortical columnar architecture depends on neuronal activity.

Columnar architecture is the hallmark of the mammalian neocortex. What determines the final dimensions of individual columns, however, remains largely unknown. Manipulations of early visual experience indicate that the segregation of eye-specific columns is a competitive process between axons serving the two eyes in primary visual cortex (*1*, *2*). Cortical target neurons detect patterns of input activity to strengthen those connections correlated with their own firing, while weakening uncorrelated afferent input. Gross disruption of postsynaptic activity supports such a correlation-based mechanism of refinement (*3*, *4*). Yet, recent reports have shown that initial clustering of individual thalamocortical arbors occurs at least a week before the critical period (*5*), leading to a suggestion that it may be largely genetically predetermined (*6*) rather than emerging from an initially overlapping configuration.

Computational models based on traditional, self-organizing principles offer specific predictions about column spacing (*7*, *8*). Local excitatory connections within cortex may spread incoming afferent activity over a certain radius, which is ultimately limited by farther-reaching inhibition. Modulating the relative balance of excitation to inhibition alters the shape of this interaction function. Activity-dependent processes acting upon narrowed or broadened central excitatory regions would ultimately

[1]Laboratory for Neuronal Circuit Development, RIKEN Brain Science Institute, 2-1 Hirosawa, Wako-shi, Saitama 351-0198, Japan. [2]W. M. Keck Foundation Center for Integrative Neuroscience, Department of Physiology, University of California–San Francisco, San Francisco, CA 94143–0444, USA.

*To whom correspondence should be addressed. E-mail: hensch@postman.riken

Materials and Methods:

Force clamp AFM.

Our single molecule force-clamp AFM was built as previously described (*1*). The instrument was upgraded with a new, three dimensional piezoelectric translator "Picocube"; P-363.3CD from Physik Instrumente (Karlsruhe, Germany). This actuator has a short range of movement (~ 6500 nm in the z axis), a very high frequency response in z axis positioning (> 7kHz), and has capacitive sensing of position with sub-nanometer resolution. The use of this piezoelectric translator was crucial for the experiments reported in this paper. We now routinely obtain about 0.5 nm resolution in measurements of the length of single proteins. Furthermore, the high resonant frequency of the device makes it possible for our analog force clamp to complete a force step in less than 3 ms and achieve slew rates that reach up to ~ 70000 nm/s. It is clear that further improvements in piezoelectric technology have the potential for improving the resolution of force spectroscopy. Another important advance was the realization that force-spectroscopy benefits from using the softest available cantilevers. This helps the feedback electronics by providing with relatively larger signals for the error amplifier. While the cantilever may have a low spring constant, the feedback mechanism compensates for any deflection by adjusting the length of the molecule and hence, the cantilever's spring constant under force feedback becomes less relevant. In all our measurements we have used 15 pN/nm cantilevers from Digital Instrument (microlevers from formerly Thermomicroscopes). Our measurements would benefit significantly from the use of softer cantilevers. The spring constant of each individual AFM cantilever was calibrated in solution prior to use as reported before (*1*).

All our experiments were done by suspending a concentrated solution of the $(Ubi)_9$ ubiquitin chains in PBS buffer at a concentration of 10-100 $\mu g\ ml^{-1}$ and allowed to adsorb onto freshly evaporated gold coverslips. The force clamp apparatus was controlled by software written in the macro language "Igor" (Wavemetrics, Oswego, Oregon). The software automated the entire operation of the spectrometer in a manner that allowed for systematic attempts to pickup single ubiquitin molecules from a well defined area of the surface of the gold-coated cover-slip. Successful pickups were recognized by the fingerprint of ubiquitin unfolding which corresponds to step increases in length of 20 nm each.

Protein Engineering.

Polyubiquitin chains were cloned and expressed as before (*2*). We cloned the $(Ubi)_9$ ubiquitin chain from a human precursor cDNA carrying nine repeats of the ubiquitin sequence. The $(Ubi)_9$ ubiquitin chains were then transformed and expressed into the E. coli recombination-defective strain BLR (DE3) (Novagene). The polyprotein, $(Ubi)_9$, was purified by Co^{2+}-affinity chromatography using a Talon resin (Clontech) and then kept at 4^o C in a solution containing 50mM sodium phosphate buffer at pH 7.0, 300 mM sodium chloride and 150 mM imidazole.

Additional data:

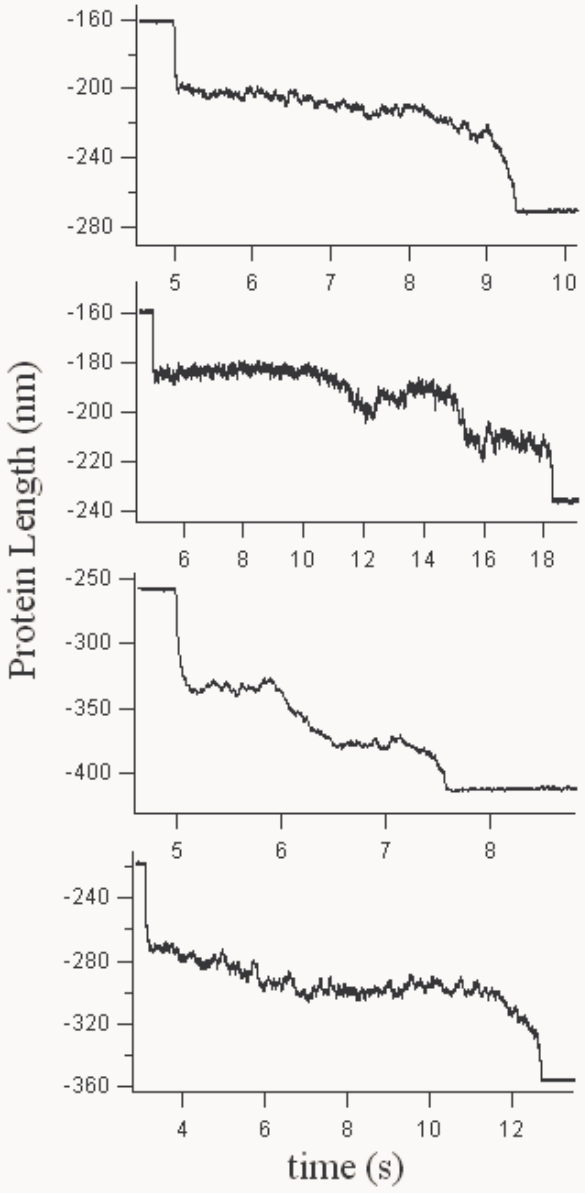

Figure S1. Set of additional folding trajectories. The figure shows four additional folding trajectories that led to full folding of the ubiquitin chain. The folding trajectories are characteristically convex and heterogeneous, however, they all show the rapid initial elastic recoil (stage 1), followed by several collapse stages. Notice the lack of stepwise shortening and the overall non-exponential, convex nature of the folding trajectories. Although the first stage is always clearly marked, the intermediate collapse stages cannot always be clearly separated and show large variations in slope at any pulling force or length. The values of the slopes varied between the slower initial stage which could be less than a nanometer per second resulting in a long lasting plateau, up to the final slope which was always the fastest in the collapse trajectories and had an average slope of 585 $\pm$ 552 nm/s (n=46).

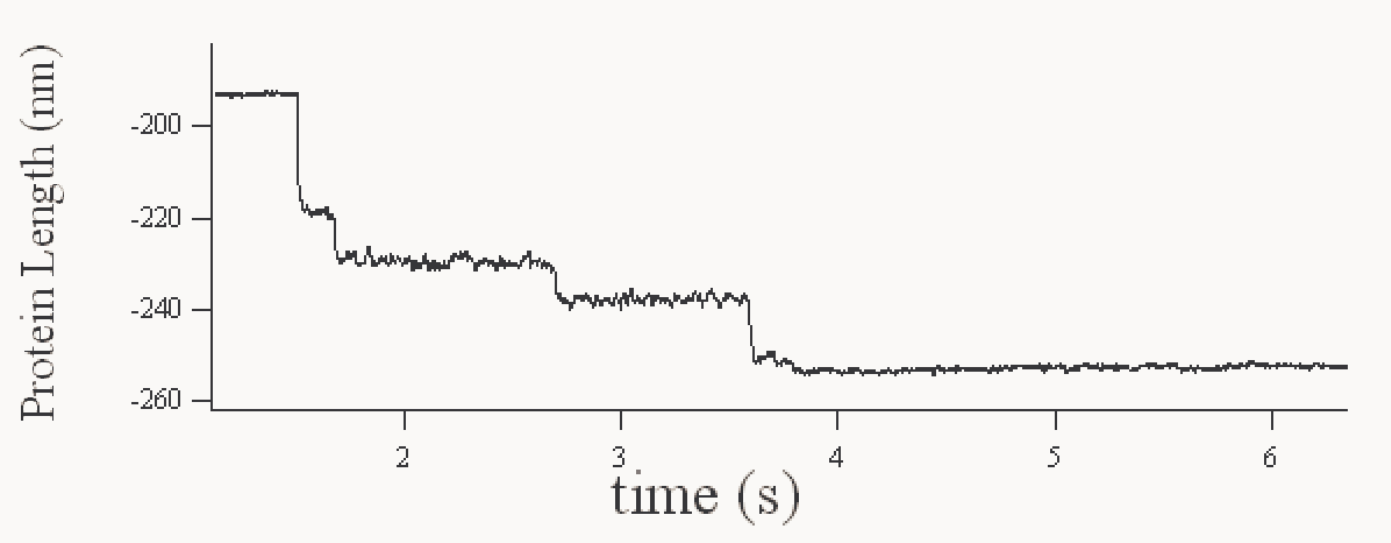

Figure S2. The only case where we have observed a ubiquitin folding trajectory composed of step-like events.

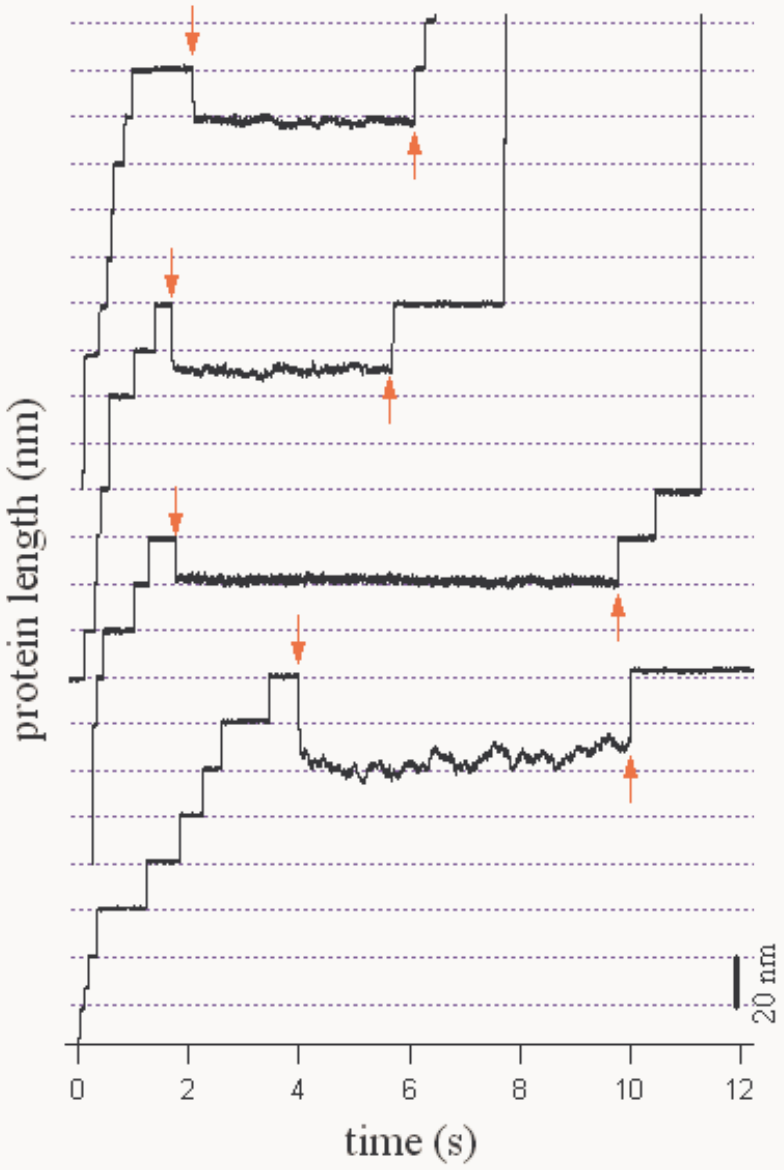

Figure S3. Folding trajectories interrupted at stage two. The figure shows a set of recordings where an initial pull at high force(100-120 pN) unfolds the ubiquitin chain resulting in an elongation of the protein in steps of 20 nm, marking each unfolding event. Upon quenching the pulling force (downward arrow), an immediate elastic recoil is observed (stage 1) after which the length of the protein fluctuates around a relatively constant value (stage 2). These traces are never observed to start on the convex trajectory of a typical folding event. Upon increasing the force again (upward arrow), we observed the length of the protein to increase back to its fully unfolded length. In 51 recordings of this type, we counted a total of 282 unfolding events and zero folding events. Hence, trajectories that are interrupted at stage 2 do not result in folding.

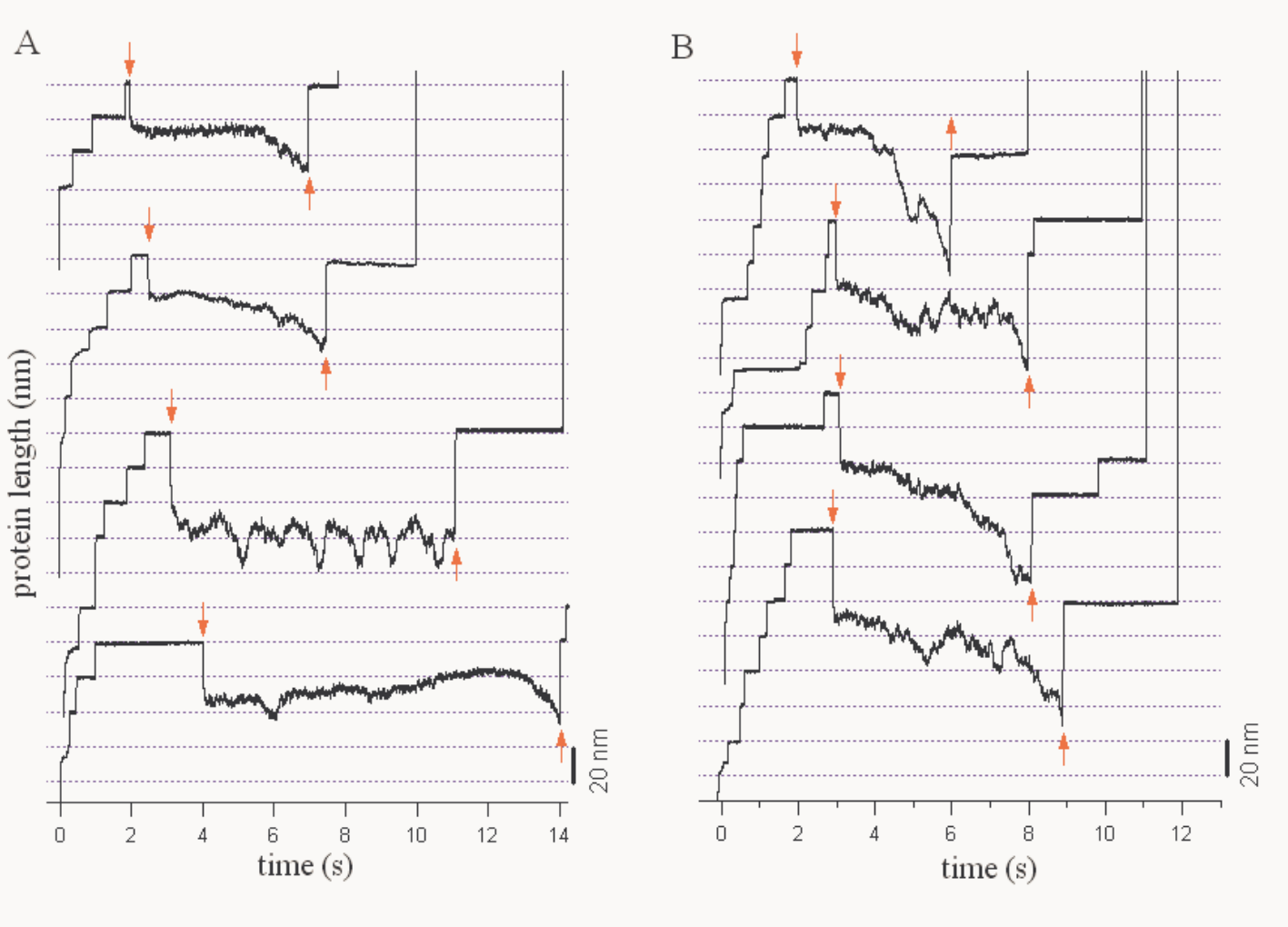

Figure S4. Folding trajectories interrupted at stage three. The figure shows a set of folding trajectories that have been interrupted by pulling back the protein at a high force before it reached its final folding step. A) These examples show typical interrupted folding trajectories. In all cases, the initial pull (100-120 pN) unfolds the ubiquitin chain resulting in an elongation of the protein in steps of 20 nm, marking each unfolding event. Relaxation of the pulling force to a low value (10-35 pN; downward arrow) resulted in a rapid initial recoil (stage 1), followed by a long stage (stage 2) and a clearly marked increased rate of collapse (stage 3). In all these cases, the folding trajectories were interrupted by pulling back to the same high force that had triggered the initial unfolding of the ubiquitin chain. Upon pulling back (upward arrow), the length of the protein jumped immediately back to its fully unfolded length. Hence, it is clear that these trajectories did not lead to folding. Of particular interest is the third recording from the top which shows repeated attempts to fold by reaching stage three of the collapse and then reverting back. When this trajectory was interrupted by pulling again at a high force, none out of the six unfolded ubiquitins had succeeded in folding. Twenty-five out of the 31 trajectories interrupted at stage 3 did not show any folding at all, like those shown in A). However, in six trajectories we observed a few folding events such as those shown in B). In all 31 trajectories interrupted at stage 3, we observed only 11 folding events out of 154 unfolding events (~7%). By contrast, in 76 folding trajectories that reached their final stage (stage four) we counted 266 folding events out of 285 unfolding events (93%).

References:

1. A. F. Oberhauser, P. K. Hansma, M. Carrion-Vazquez, J. M. Fernandez, *Proc Natl Acad Sci U S A* **98**, 468 (2001).
2. M. Carrion-Vazquez *et al.*, *Nat Struct Biol* (2003).